AD-A056 850 TEXAS A AND M UNIV COLLEGE STATION DEPT OF PHYSICS F/G 3/1
FURTHER STUDIES OF SUNLIGHT GLITTER ON A WIND-RUFFLED SEA,(U)
JUN 78 J A GUINN, G N PLASS, G W KATTAWAR N00014-75-C-0537
UNCLASSIFIED TR-12 NL

1 OF 1
AD A056850

END
DATE FILMED
9-78
DDC

LEVEL II

Further Studies of Sunlight Glitter on a Wind-Ruffled Sea

By

John A. Guinn, Jr., Gilbert N. Plass and George W. Kattawar

Report No. 12

TR-12

The research described in this report was

funded by

The Ocean Science and Technology Division

of the

Office of Naval Research

Contract N00014-75-C-0537

Department of Physics

Texas A&M University

College Station, Texas 77843

15 Jan 78

June 15, 1978

40 pp.

This report has been submitted to Applied Optics for publication.

400 771

Further Studies of Sunlight Glitter on a Wind-Ruffled Sea

John A. Guinn, Jr., Gilbert N. Plass, and George W. Kattawar

Abstract

Time-averaged intensities are computed for the glitter pattern of sunlight on a wind-ruffled sea. In the present work the azimuthally asymmetric form of the wave-slope distribution measured by Cox and Munk is used, so that the glitter pattern depends on the wind direction as well as magnitude. Results are calculated for both a clean ocean surface and one covered with an oil film. The glitter pattern is quite different with the oil film due to the quieting action of the oil on the waves, the greater reflectivity of the surface when oil is on the surface, and the larger values of polarization for the reflected light at most typical angles in the glitter pattern. These effects are illustrated and discussed as possible methods for the detection of oil slicks. The glitter pattern observed at satellite altitudes is also calculated.

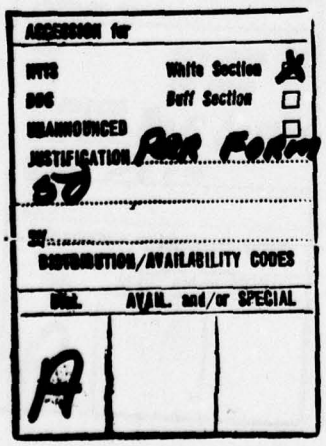

The authors are with Texas A&M University, Physics Department, College Station, Texas 77843. Present address of John A. Guinn, Jr.: Radiation Research Associates, Inc., Fort Worth, Texas 76107.

I. Introduction

Glitter, the pattern of coruscations one can see on a wind-ruffled water surface that is illuminated by a strong source, is a commonplace phenonmenon of the type that M. Minnaert particularly enjoyed investigating. Although frequently observed and often recorded -- sometimes inaccurately -- by artists, little thought has been devoted to glitter pattern morphology and its causes. The existence of a glitter pattern on a sunlit sea is indeed not surprising, but it is not entirely obvious why the pattern should assume a particular configuration under a given set of circumstances. Through some basic geometrical considerations, Hulburt[1] related the solar elevation angle and what he called the effective maximum wave slope, a measure of sea roughness, to the width of the glitter pattern. Minnaert[2,3] added considerable detail to the analysis of the problem; his observations are discussed further as they apply to these results. Certain geometrical insights regarding glitter and related comments pertaining to the distortion of the shapes of objects reflected in a wind-ruffled water surface have been provided by Tricker[4] and Goodell[5]. Gambling[6] has studied sun glitter in the infrared spectral region.

Plass et al[7] have calculated the time-averaged intensities for the glitter pattern of sunlight on a wind-ruffled sea. Isopleths drawn on graphs simulate glitter-pattern photographs. The pattern is computed from the wave-surface orientation required for direct reflection from the source to the observer; the intensity is computed from the probability of occurrence of this orientation, as determined from the Cox-Munk distribution, together with the fraction of the radiation reflected at that particular angle of incidence. The curvature of the earth is taken into account.

II. Method of Calculation

The glitter is composed of the many bright, instantaneous points of light created on the water surface by local surface orientations which are momentarily appropriate for the direct reflection of the source into the eye of the observer. The brightness of each glint depends on the reflection coefficient of the reflection which produces the glint; the reflection coefficient in turn depends on the angle of incidence of the reflection. The perceived (time-averaged) brightness of a particular region of the glitter pattern is a consequence of the brightness of individual glints and their frequency of occurrence. The frequency of occurrence of highlights at a particular location on the water surface depends on the local surface orientation required to produce the highlights and the nature of the prevailing distribution of surface orientations. A glitter-pattern model therefore must assume a surface-orientation distribution.

In the present work the general procedure described in Ref. 7 is followed, but the new calculations take into account the complete, azimuthally asymmetric form of the wave-slope distribution measured by Cox and Munk[8]. A bivariate normal distribution having different standard deviations for the upwind (σ_u) and crosswind (σ_c) components is used. This distribution is modified, to produce a Gram-Charlier distribution, by multiplying the bivariate normal density function by a sum of products of Hermite polynomials. The density function is therefore

$$p(z_c,z_u) = [G(a,b)/2\pi\sigma_c\sigma_u] \exp[-\tfrac{1}{2}(a^2+b^2)]. \qquad (1)$$

In Eq. (1), z_c and z_u are the crosswind and upwind components, respectively, of the wave slope, $a = z_c/\sigma_c$, and $b = z_u/\sigma_u$. $G(a,b)$, a sum of products of

Hermite polynomials, is the Gram-Charlier sum, which can be written

$$G(a,b) = 1 - \tfrac{1}{2}c_{21}(a^2 - 1)b - c_{03}(b^3 - 3b)/6 + c_{40}(a^4 - 6a^2 + 3)/24$$
$$+ \tfrac{1}{4}c_{22}(a^2 - 1)(b^2 - 1) + c_{04}(b^4 - 6b^2 + 3)/24 + \ldots \qquad (2)$$

Notice that two of the terms are asymmetric about the origin in the upwind direction. The coefficients of the sum, experimentally determined by Cox and Munk[8], are given in Table I for a clean water surface and for a surface covered by an oil slick.

The absence of a cross-product term in the argument of the density-function exponential is due to the choice of the upwind and crosswind directions as the coordinate axes. There is, in other words, no statistical correlation, in the absence of the Gram-Charlier sum, between the upwind and crosswind components of the wave orientations.

The data of Cox and Munk[8] (as well as those of Duntley[9] who achieved similar results) indicate a linear relationship between the upwind and crosswind variances and the wind speed. The Cox and Munk results for a clean water surface are

$$\sigma_c^2 = 0.003 + 0.00192W$$
and (3)
$$\sigma_u^2 = 0.000 + 0.00316W,$$

while for a surface covered by an oil slick

$$\sigma_c^2 = 0.003 + 0.00084W$$
and (4)
$$\sigma_u^2 = 0.005 + 0.00078W,$$

where W is measured in m/sec at a height of 12.5 m above the sea surface.

For the clean surface the crosswind constant term dominates for $W < 2.42$ m/sec, while $\sigma_u > \sigma_c$ for greater wind speeds. For the slick surface $\sigma_u > \sigma_c$ for $W < 33.3$ m/sec, which completely covers the range of wind speeds considered here. Thus the asymmetries have the same sense for 2.42 m/sec $< W <$ 33.3 m/sec and the opposite sense for $W < 2.42$ m/sec. However, Eqns. (3) and (4) show that the upwind-crosswind asymmetry is very small for the slick surface compared to the clean surface. The equations also show the smoothing effect of the oil slick.

The graphs presented here represent the projection of the sea surface onto an inclined plane placed in front of the observer and simulate the image that would be recorded on a photographic plate. Each point on the plane corresponds uniquely to a point on the sea surface (except for points which project above the horizon). The correspondence is determined by requiring the lines of projection to meet at the observer. Calculations were made of glitter-pattern intensity (time-averaged), polarization, and certain other quantities for points in a rectangular grid on the inclined plane. For each of these points the corresponding sea-surface location was determined, and from that the surface orientation required for a direct reflection of the source to the observer calculated. The required surface inclination and azimuth were then applied to the density function already discussed to calculate the probability of occurrence of the surface orientation in question. This probability then became a factor in the calculation of the glitter intensity at the grid point, as did the coefficient of reflection determined from the angle of incidence of the light from the source on the surface element of correct orientation. The computed quantities assigned to the grid points were used to generate the contour plots shown.

The coordinate system used for the graphs is the same as that used in Ref. 7, which provided a detailed description. Very briefly, the graphs represent a projection of the glitter pattern and a sea-surface rectangular coordinate system onto a plane inclined so that it is perpendicular to the line connecting the observer with the center of the vertical axis of the graph. Since these graphs generally are not bilaterally symmetric, as were those of Ref. 7, both sides of the principal plane are represented. Wind direction is measured clockwise from the solar azimuth.

For a clean water surface the coefficient of reflection, for a single interface, is simply determined from the angle of incidence and the index of refraction of sea water (assumed to be 1.338). The coefficient of reflection is slightly more complicated when there is a double interface, as is the case when the sea surface is contaminated with an oil slick. Let R_1 and R_2 represent the fractional intensities reflected at the first and second interfaces, respectively. If the interfaces are assumed parallel, a simple calculation shows that the total reflected intensity including all orders of multiple reflection within the oil film is

$$R = R_1 + R_2(1 - R_1)^2 / (1 - R_1R_2). \qquad (5)$$

Interference effects and absorption and scattering within the layer are neglected.

The coefficient of reflection for a single interface (air-water) is shown in Fig. 1 (solid curve); for a double interface (air-layer-water, where the layer, representing an oil slick, has an index of refraction of 1.5) it is shown as a broken line with solid circles. A similar double layer with oil with index of refraction of 1.6 is shown as a dashed line. The parallel component for water alone is zero at the Brewster angle, 53.23°, but with a

double interface the parallel component never quite reaches zero, as shown in the inset on the graph. For oil with n = 1.5, the minimum value for the parallel component occurs at an angle of incidence of 56.6° and the maximum polarization is 0.9909. When n = 1.6, the corresponding angle is 58.5° and the maximum polarization is 0.9824. The curve for the latter case is not shown in the inset as it is off scale.

The polarization of the reflected radiation for the same three cases is shown in Fig. 2 with the assumption that the source is unpolarized.

III. Intensities for Observer Near Surface

The variation in the structure of the glitter pattern with changes in the wind direction are illustrated in this section. Figs. 3, 4, and 5 are parametrically identical except for wind direction. Each figure represents a clean surface illuminated by a source (at infinite distance, i.e. the sun) at 30° elevation, ruffled by a 10 m/sec wind, and observed from a height of 5 m above the sea surface. The wind directions are 0°, 45°, and 90°, respectively. The principal plane corresponds to the centerlines of these figures and wind directions are measured from this line. The coordinates θ_x and θ_y are explained in Ref. 7. The numbers associated with each contour line give the logarithm to the base 10 of the intensity of the time-averaged radiance.

Though the range of intensity is essentially the same in each case, the effect of varying wind direction can be clearly seen in the morphological differences among these figures. The U-shaped contours of Fig. 3 (wind from the solar azimuth) give way to V-shaped contours in Fig. 5 (direct crosswind). The brightest contours of Fig. 5 are much closer to the triangular forms noted by Minnaert[3] than any of the contours generated by the azimuthally symmetric

wave-slope distributions of Ref. 7. Fig. 5 is bilaterally symmetric because of the small magnitude of c_{03}, the coefficient of the antisymmetric upwind terms of the Gram-Charlier sum, but the contours of Fig. 4 are skewed noticeably to the right by a diagonal wind. Because all crosswind terms are symmetric, Fig. 3 displays the bilateral symmetry characteristic of all cases for which the wind is from the solar azimuth.

The slick-surface counterparts to Figs. 3 and 5 are Figs. 6 and 7, respectively. All parameters correspond to the earlier figures, except that the surface is assumed to be covered with an oil layer with an index of refraction of 1.5. Waves of lesser inclination are favored when the slick is present, hence the contours are drawn in, and the brightest spot is no longer on the horizon. The intensity at the horizon is not greatly diminished from the maximum, particularly in the case of Fig. 6; the intensity difference is only 21% between the maximum and the brightest contour that meets the horizon. The glitter pattern would be a narrow, bright streak extending downward from the horizon. The contrast between the maximum and the horizon is somewhat greater in Fig. 7, the intensity difference with respect to the maximum being 44% at the brightest contour to meet the horizon; the glitter pattern is noticeably broader than the one in Fig. 6.

The next two cases were calculated for a 30° source elevation, an observer at a height of 5 m, and a 1 m/sec wind from a 45° azimuth. The only difference between the two is that Fig. 8 represents a clean surface and Fig. 9 a slick surface. The opposite skewing of the isopleths, despite the common wind direction for the two graphs, is due to the fact that at 1 m/sec the crosswind variance dominates for the clean surface, while the opposite is the case for the slick surface.

An oblique wind does not assure bilateral asymmetry. Fig. 10 (5 m

observer height, 5° sun elevation, oil slick surface, 10 m/sec wind speed, and 45° wind azimuth) is very nearly symmetric because the upwind and crosswind variances are approximately the same for this wind speed.

IV. High-Altitude Observer

The next seven figures represent the calculated appearance of the glitter pattern to an observer at a height of 150 km. In each case the sun is 30° above the horizontal reference plane. The horizon can be seen as the uppermost curve in each figure. A wind speed of 10 m/sec was used for Figs. 11-13. Figs. 11 and 12 represent a clean surface, while Fig. 13 is for an oil slick surface. In Fig. 11, for which the wind direction is 45°, the asymmetry is quite clear, with the bright spot on the horizon distinctly to the right of the principal plane. A wind shift to 90° (Fig. 12) eliminates the asymmetry and, because the crosswind variance is less than the upwind variance, moves the bright spot away from the horizon. It also produces a shield, one of the distinctive shapes generated by certain combinations of parameters. In Fig. 13 the wind azimuth is still 90°, but an oil slick has been added. This change shifts the bright region farther below the horizon and splits the brightest spot into two parts.

Figs. 14-17 were generated assuming a 1 m/sec wind speed, a 150 km observer height, and a 30° solar elevation. The oil slick model was used for Figs. 16 and 17. The wind azimuth is 0° for Figs. 14 and 16 and 90° for Figs. 15 and 17. At 1 m/sec the crosswind standard deviation dominates for the clean surface, while for the surface with an oil slick the upwind standard deviation is larger. (The ratio of the larger figure to the smaller is roughly 1.5 in each case.) As a consequence the clean-surface contours are broadest when the wind azimuth is 0°, while contours for the slick surface

are broadest for a 90° wind azimuth. Thus, the heart-shape of Fig. 14 (clean surface) becomes the tear drop of Fig. 16 (oil slick), while the tear drop of Fig. 15 becomes the heart-shape of Fig. 17 (oil slick).

Figs. 18 and 19 (for which the Gram-Charlier sum was not used) were calculated for a nearby source. In both cases the wind speed is 10 m/sec, the wind azimuth is 45°, the observer height is 5 m, the source is horizontally displaced 100 m from the observer, and there is no oil slick. The source for Fig. 18 is at a height of 62.74 m, and that for Fig. 19 is 13.75 m high. The higher source has an apparent elevation angle of 30° as seen from the observer's position, and the apparent elevation angle of the lower source is 5°. The slanting pattern of Fig. 18 is somewhat like that of Fig. 18 of Minneart's book (Ref. 3, p. 22), which depicts the glitter pattern of a lamp across a canal. It is particularly apparent in Fig. 19 that the intensity drops off very rapidly near the horizon. This is due to very high wave inclinations required for reflection toward the observer for waves on the far side of the source.

V. Polarization

The source is assumed to be unpolarized. The degree of polarization induced by reflection is a function of the angle of incidence at each grid point. The wind speed is irrelevant for polarization since the effect depends only on the angle of incidence at the wave facet for each reflection. The probability of occurrence of the required wave slope does not enter into the calculation of the polarization, although the radiation obviously could not be observed if this probability is too small. Fig. 20 shows the isopleths of degree of polarization expressed in percent for a source displaced 100 m horizontally from the observer, a source height of 62.74 m, an observer

height of 5 m, and a clean water surface. There is a large region in which the reflected light is strongly polarized around the line for which the observed light is 100% polarized. This completely polarized light is reflected from the water surface at the Brewster angle of 53.23° (for n = 1.338). When the sun is the source (at an effective infinite distance) the polarization drops from the Brewster angle to the horizon (see Figs. 22 and 23 of Ref. 7). On the other hand, when the source is at a finite distance, the polarization first decreases toward the horizon and then increases to another maximum, as the light is once again reflected from the wave facet at the Brewster angle. For the case shown in Fig. 20, the first Brewster angle is observed at 50.19° from the vertical; this light is reflected from wave facets making an angle of 3.04° to the horizontal. For the second Brewster angle the corresponding angles are 86.28° and 33.05°, respectively.

Figure 21 is parametrically the same as Fig. 20 except that an oil slick has been added. Several changes are evident. As discussed in Sect. II, the maximum polarization for an oil slick with n = 1.5 is 99.09% for an angle of incidence of 56.6°. A comparison of Figs. 20 and 21 shows the decreased value of the polarization at the maximum when an oil slick is present as well as the displacement of this maximum toward the horizon. For the oil slick case, the observer must look at 57.44° from the vertical to observe the light reflected at the first Brewster angle; this light is reflected from wave facets making an angle of 0.84° to the horizontal. For the second Brewster angle the corresponding angles are 85.76° and 29.15°, respectively. Another difference between the two figures is the larger value of the polarization for the oil slick case in the large region between the two Brewster angles. In this region the angle of incidence of the light on the wave facets is greater than the Brewster angle. Fig. 2 shows that the polarization for a

given angle of incidence is greater for the oil slick case than for clean water for this range of angles.

VI. Possible Detection of Oil Slicks

Several possible methods for the detection of oil slicks are suggested by these results. A measurement of the polarization of the reflected radiation in the brightest part of the glitter pattern would show a slight decrease in the maximum polarization at the Brewster angle (99.09% for oil slick instead of 100% for clean water in the example considered in Sect. V); a shift of the Brewster angle toward the horizon when the oil slick is present (by 7.25° in the example); higher polarization values in the broad region from near the Brewster angle to angles near the horizon (polarization about 5% higher in this region for the oil slick in the example). The second Brewster angle discussed in Sect. V is only observed for sources at finite distances; the differences between a clean and oil slick surface are less in this case and would be more difficult to observe. The contrast in the polarization measurements for adjacent regions of the ocean with and without an oil slick should be relatively easy to measure. The great advantage of measuring the polarization is that the value observed at a given angle is independent of the sea state; of course the probability of a given wave slope must be large enough to reflect measurable light to the observer.

Oil slicks can also be observed by the changes in the intensity of the reflected light as discussed in Sect. III and IV. The main effects come from an increase in the reflectivity due to the higher index of refraction of oil than of water and to the decreased probability of higher wave slopes when an oil slick is present. The resulting changes in the intensity of the reflected light in the glitter pattern as shown in the figures suggest many

possibilities for observing the slicks.

All of the calculations discussed so far assume that geometrical optics applies to this problem. Effects due to the wave nature of light also can be prominent with an oil film. The many colors in the light reflected form such a film are well known. These occur as the light at a particular wavelength reflected from the top surface of the film interferes either constructively or destructively with the light reflected from the oil-water surface. Light form a tuneable laser reflected from an oil slick should show maxima and minima as the wavelength is varied, corresponding to these interference effects. Such maxima and minima would be a clear signature of an oil slick, as they do not exist for a clean water surface.

VII. Conclusion

The results of the glitter calculations show how the pattern varies with wind direction as well as wind velocity. Both the shape of the glitter pattern and the intensity of the reflected light change appreciably when an oil slick is on the water and this fact can be used to locate such slicks. The polarization of the light in the glitter pattern is also appreciably changed when an oil slick is on the surface. Results are shown for an observer just above the ocean surface as well as at satellite altitudes. The radiation in the glitter pattern is an important component of the upwelling radiant energy above an ocean.

This research was supported by the Office of Naval Research through contract N00014-75-C0537.

References

1. E. O. Hulburt, J. Opt. Soc. Am. 24, 35 (1934).
2. M. Minnaert, Physica 9, 925 (1942).
3. M. Minnaert, The Nature of Light and Colour in the Open Air (Dover, New York, 1954), pp. 15-26.
4. R. A. R. Tricker, Bores, Breakers, Waves and Wakes (American Elsevier, New York, 1965), pp. 240-246.
5. J. B. Goodell, Appl. Opt. 10, 223 (1971).
6. D. J. Gambling, Infrared Phys. 15, 149 (1975).
7. G. N. Plass, G. W. Kattawar, and J. A. Guinn, Jr., Appl. Opt. 16, 643 (1977).
8. C. Cox and W. Munk, J. Opt. Soc. Am. 44, 574 (1954).
9. S. Q. Duntley, J. Opt. Soc. Am. 44, 574 (1954).

Table I. Gram-Charlier Coefficients

Coefficient	Value (W = wind speed in m/sec)	
	Clean surface	Oil slick
c_{21}	0.01 - 0.0086W	0.00
c_{03}	0.04 - 0.033W	0.02
c_{40}	0.40	0.36
c_{22}	0.12	0.10
c_{04}	0.23	0.26

Captions for Figures

Fig. 1. Reflectivity as a function of the angle of incidence (θ) for a clean water surface (solid curve); oil film (n = 1.5) on water (dashed curve with solid circles); oil film (n = 1.6) on water (dashed curve). Note the different scales for the left and right half diagrams. In each case the lower curve is for the parallel component, while the upper curve is for the perpendicular component. The inset shows the reflectivity of the parallel component near the Brewster angle.

Fig. 2. The polarization of the reflected radiation as a function of the angle of incidence (θ) for a clean water surface (solid curve); oil film (n = 1.5) on water (dashed curve with solid circles); oil film (n = 1.6) on water (dashed curve).

Fig. 3. Intensity isopleths for a source elevation of 30°, an observer height of 5 m, and a wind from a 0° azimuth at 10 m/sec. The numbers beside the curves give the logarithm of the intensity to the base 10. Maximum $\log_{10}$ intensity is -4.018. The coordinates are explained in the text and in Ref. 7.

Fig. 4. Intensity isopleths for a source elevation of 30°, an observer height of 5 m, and a wind from a 45° azimuth at 10 m/sec. Maximum $\log_{10}$ intensity is -4.102.

Fig. 5. Intensity isopleths for a source elevation of 30°, an observer height of 5 m, and a wind from a 90° azimuth at 10 m/sec. Maximum $\log_{10}$ intensity is -4.215.

Fig. 6. The same as Fig. 3, except that an oil slick is added. Maximum $\log_{10}$ intensity is -4.211.

Fig. 7. The same as Fig. 5, except that an oil slick is added. Maximum $\log_{10}$ intensity is -4.250.

Fig. 8. Intensity isopleths for a clean surface, a source elevation of 30°, an observer height of 5 m, and a wind from a 45° azimuth at 1 m/sec. Maximum $\log_{10}$ intensity is -4.009.

Fig. 9. The same as Fig. 8, except that an oil slick is added. Maximum $\log_{10}$ intensity is -3.911.

Fig. 10. Intensity isopleths for an oil slick surface, a source elevation of 5°, an observer height of 5 m, and a wind from a 45° azimuth at 10 m/sec. Maximum $\log_{10}$ intensity is -2.781.

Fig. 11. Intensity isopleths for a clean surface, a source elevation of 30°, an observer height of 150 km, and a wind from a 45° azimuth at 10 m/sec. Maximum $\log_{10}$ intensity is -4.661. The top curve is the horizon.

Fig. 12. Intensity isopleths for a clean surface, a source elevation of 30°, an observer height of 150 km, and a wind from a 90° azimuth at 10 m/sec. Maximum $\log_{10}$ intensity is -4.763. The top curve is the horizon.

Fig. 13. The same as Fig. 12, except that an oil slick is added. Maximum $\log_{10}$ intensity is -4.366. The top curve is the horizon.

Fig. 14. Intensity isopleths for a clean surface, a source elevation of 30°, an observer height of 150 km, and a wind from a 0° azimuth at 1 m/sec. Maximum $\log_{10}$ intensity is -4.112. The top curve is the horizon.

Fig. 15. Intensity isopleths for a clean surface, a source elevation of 30°, an observer height of 150 km, and a wind from a 90° azimuth at 1 m/sec. Maximum $\log_{10}$ intensity is -4.101. The top curve is the horizon.

Fig. 16. The same as Fig. 14, except that an oil slick is added. Maximum $\log_{10}$ intensity is -3.985. The top curve is the horizon.

Fig. 17. The same as Fig. 15, except that an oil slick is added. Maximum $\log_{10}$ intensity is -4.000. The top curve is the horizon.

Fig. 18. Intensity isopleths for a source displaced 100 m horizontally from the observer, a source height of 62.74 m, an observer height of 5 m, a clean surface, and a wind from a 45° azimuth at 10 m/sec. Maximum $\log_{10}$ intensity is -4.877.

Fig. 19. The same as Fig. 18, except that the source height is 13.75 m. Maximum $\log_{10}$ intensity is -3.730.

Fig. 20. Isopleths of degree of polarization (percent) for a source displaced 100 m horizontally from the observer, a source height of 62.74 m, an observer height of 5 m, and a clean surface.

Fig. 21. The same as Fig. 20, except that an oil slick is added.

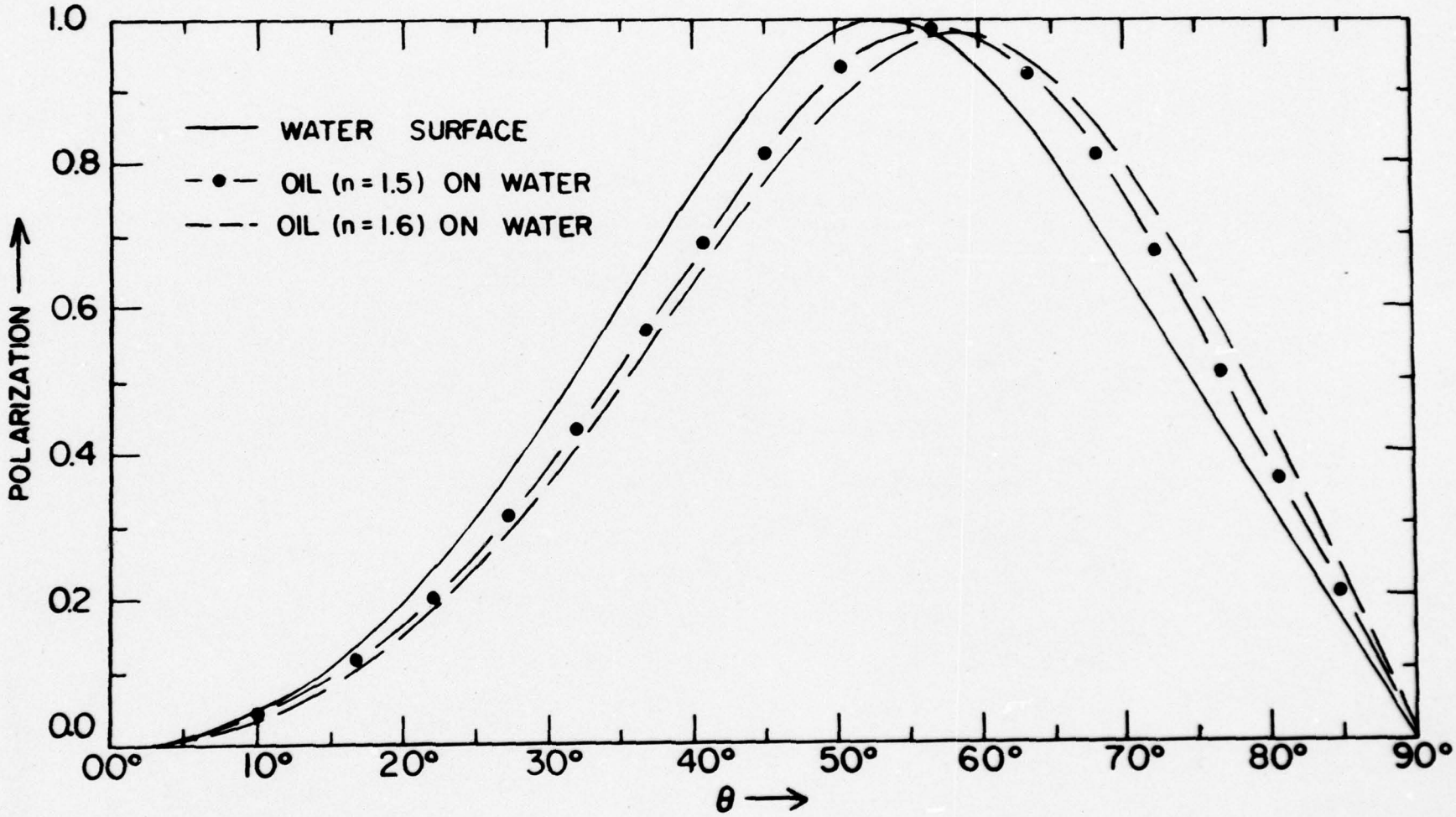
1.0
0.8
0.6
0.4
0.2
0.0
POLARIZATION
WATER SURFACE
OIL (n = 1.5) ON WATER
OIL (n = 1.6) ON WATER
00°
10°
20°
30°
40°
50°
60°
70°
80°
90°
θ

Figure 1

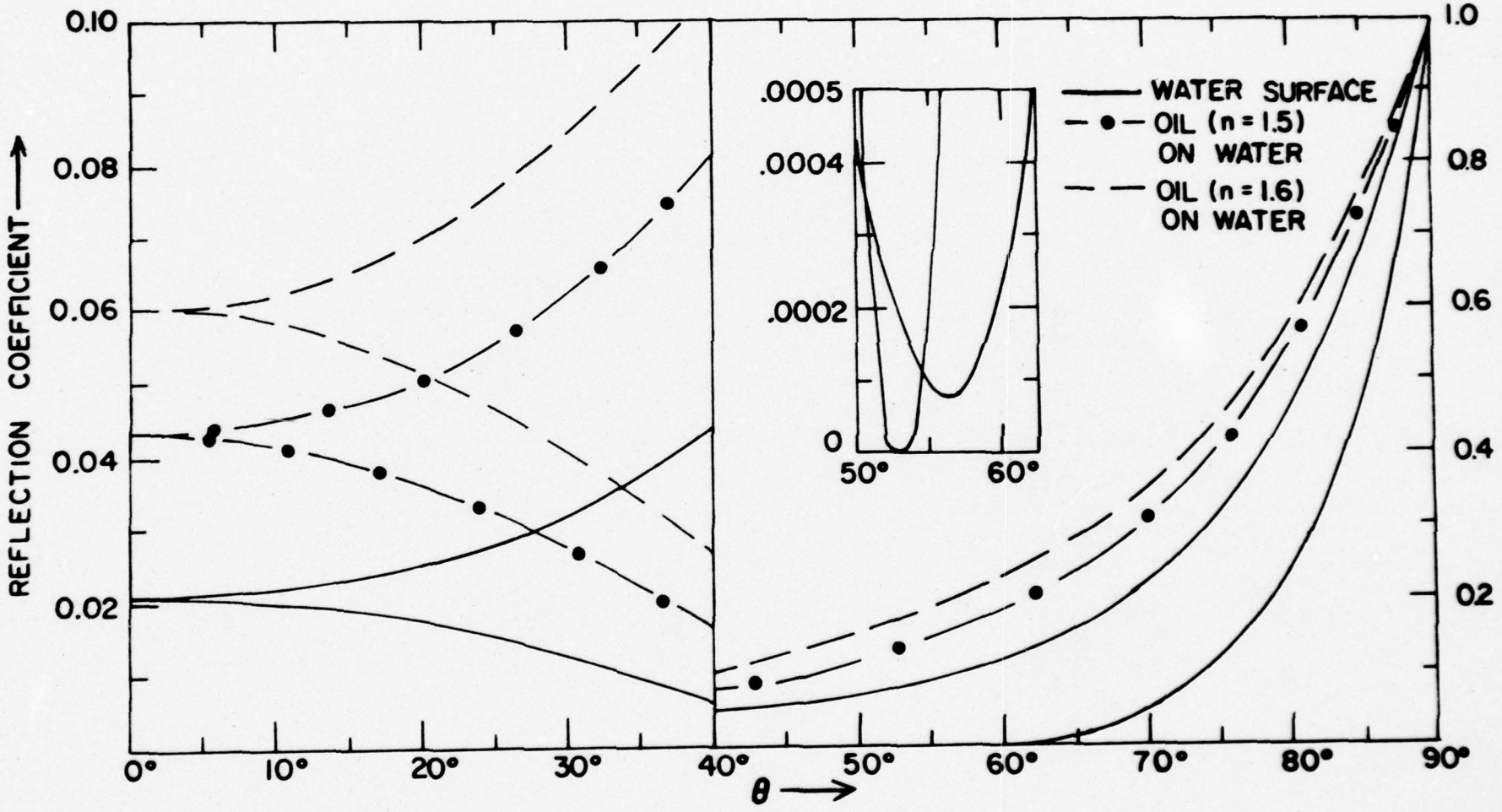
REFLECTION COEFFICIENT
0.10
0.08
0.06
0.04
0.02
.0005
.0004
.0002
0
50°
60°
WATER SURFACE
OIL (n = 1.5) ON WATER
OIL (n = 1.6) ON WATER
1.0
0.8
0.6
0.4
02
0°
10°
20°
30°
40°
50°
60°
70°
80°
90°
θ

Figure 2

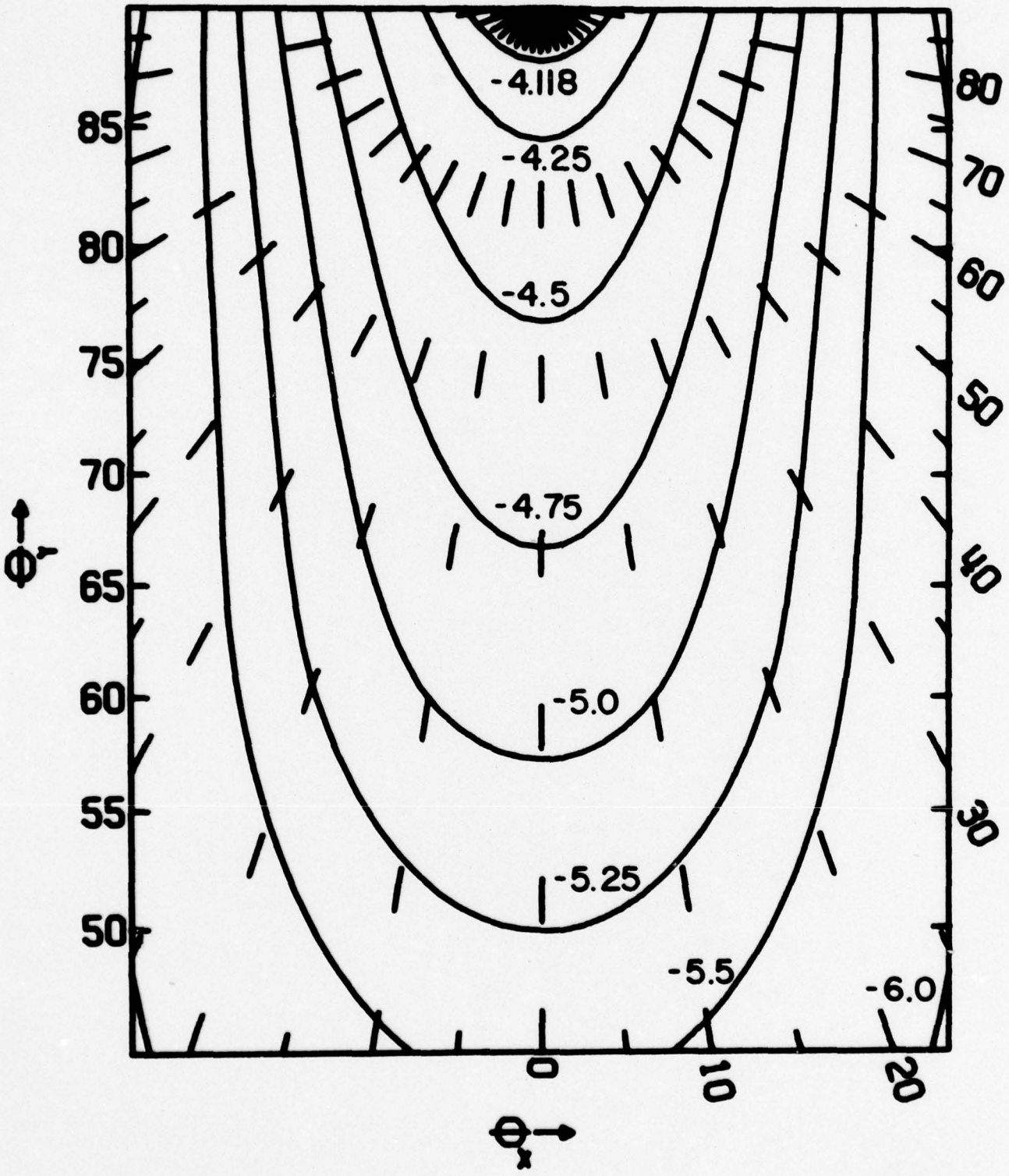
-4.118
-4.25
-4.5
-4.75
-5.0
-5.25
-5.5
-6.0
85
80
75
70
65
60
55
50
80
70
60
50
40
30
0
10
20
Φ_y
Θ_x

Figure 3

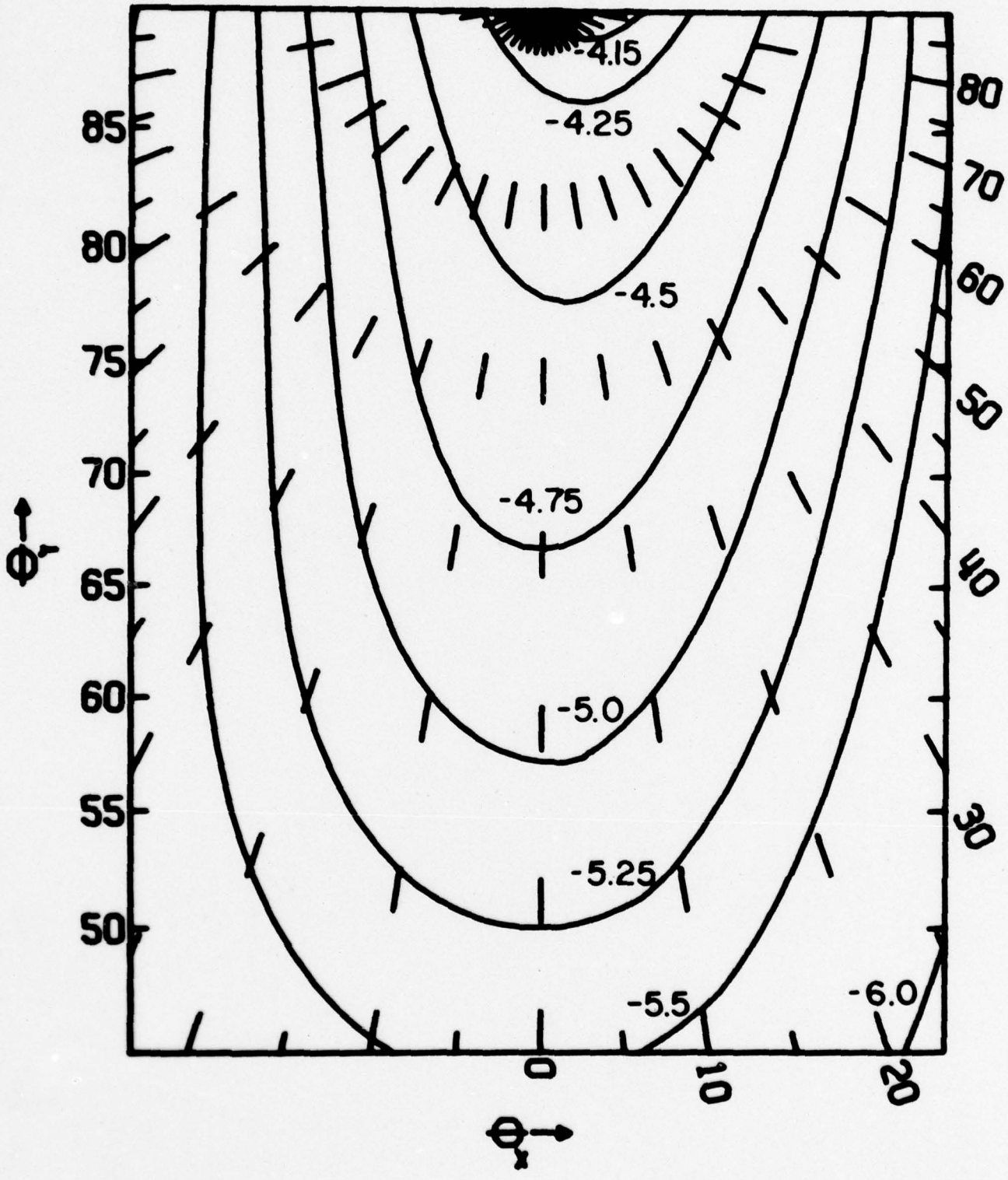
-4.15
-4.25
-4.5
-4.75
-5.0
-5.25
-5.5
-6.0
85
80
75
70
65
60
55
50
80
70
60
50
40
30
0
10
20
Φ
θ

Figure 4

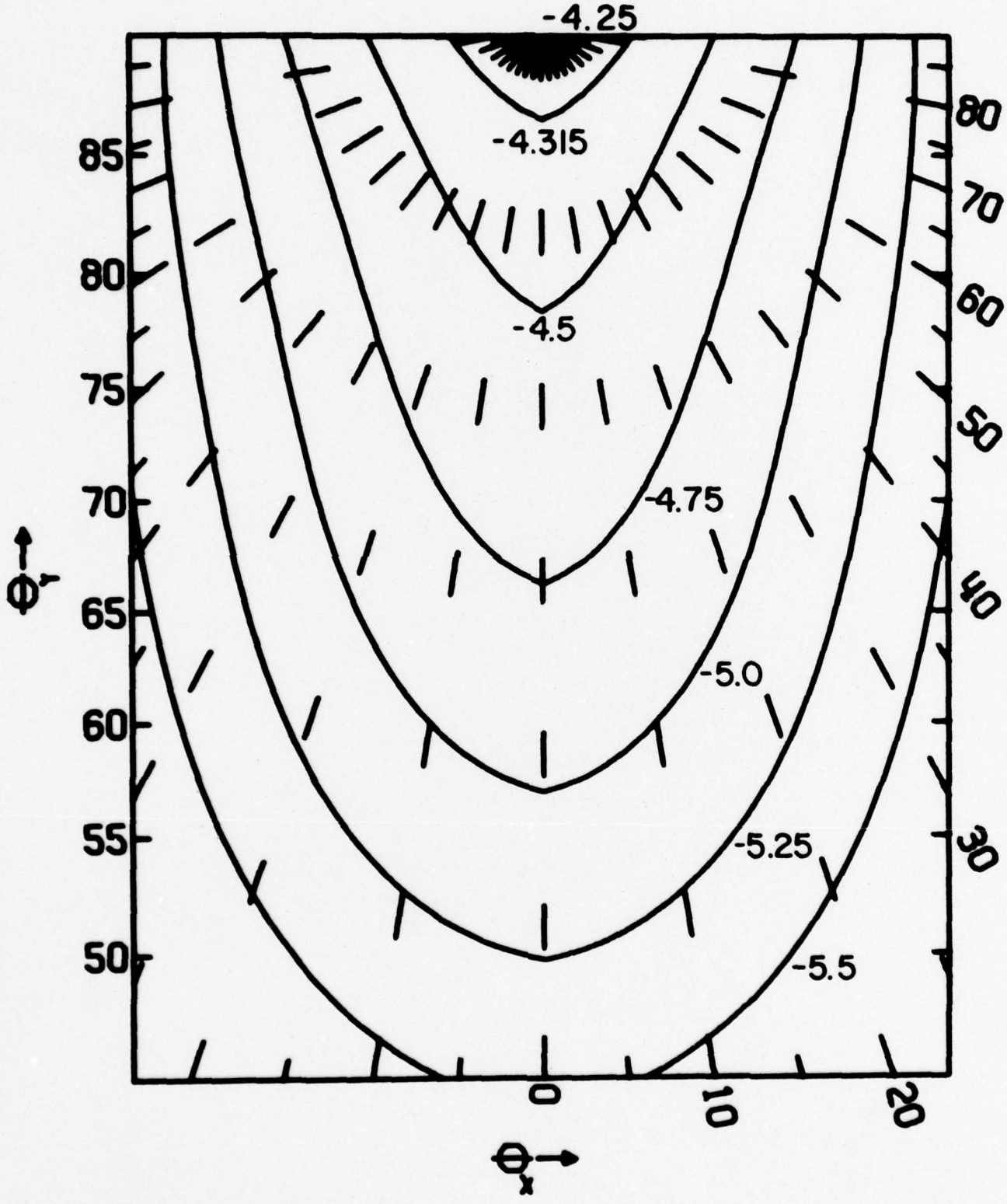
-4.25
-4.315
-4.5
-4.75
-5.0
-5.25
-5.5
85
80
75
70
65
60
55
50
80
70
60
50
40
30
0
10
20
Φ_Y
θ_X

Figure 5

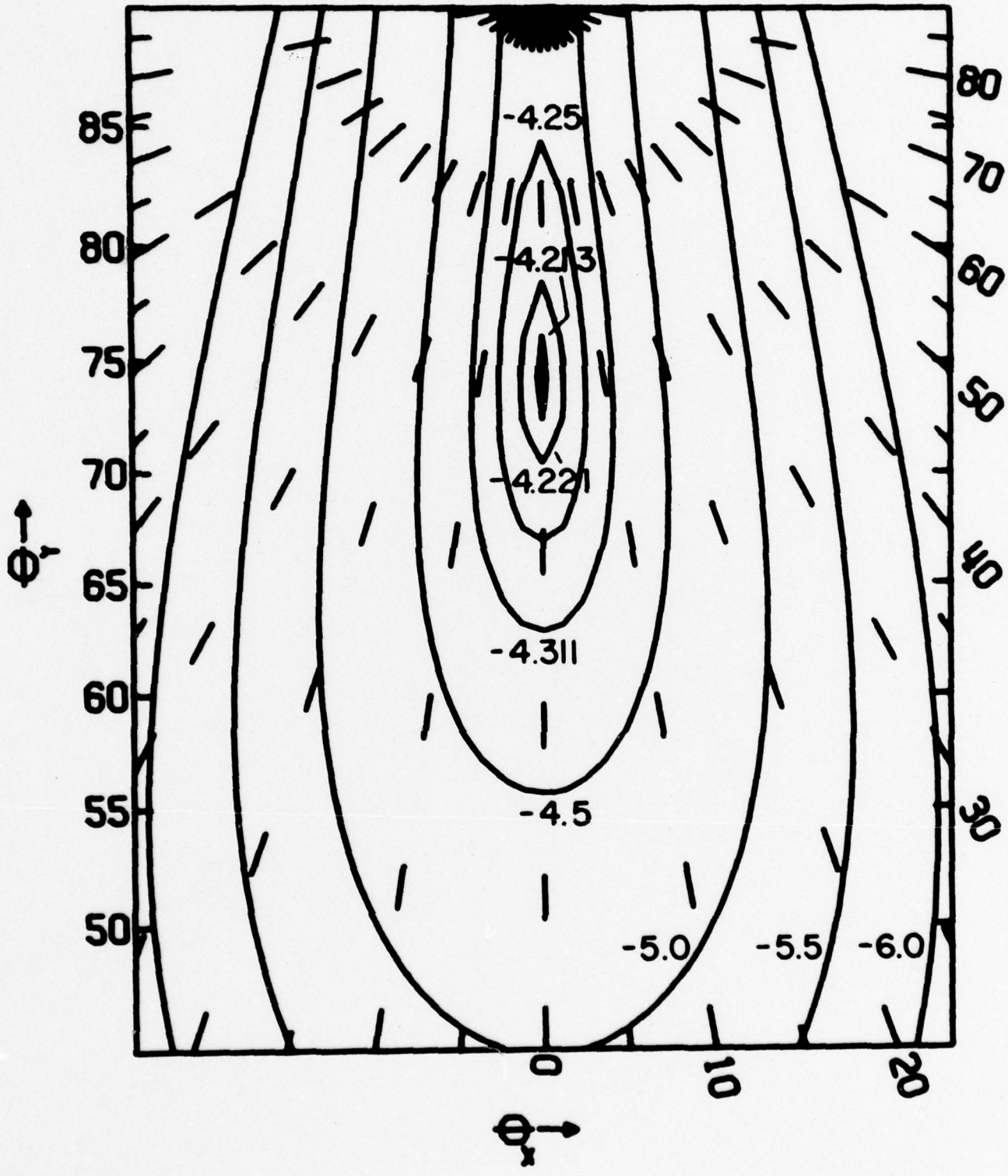
-4.25
-4.213
-4.221
-4.311
-4.5
-5.0
-5.5
-6.0
85
80
75
70
65
60
55
50
80
70
60
50
40
30
0
10
20
Φ
θ

Figure 6

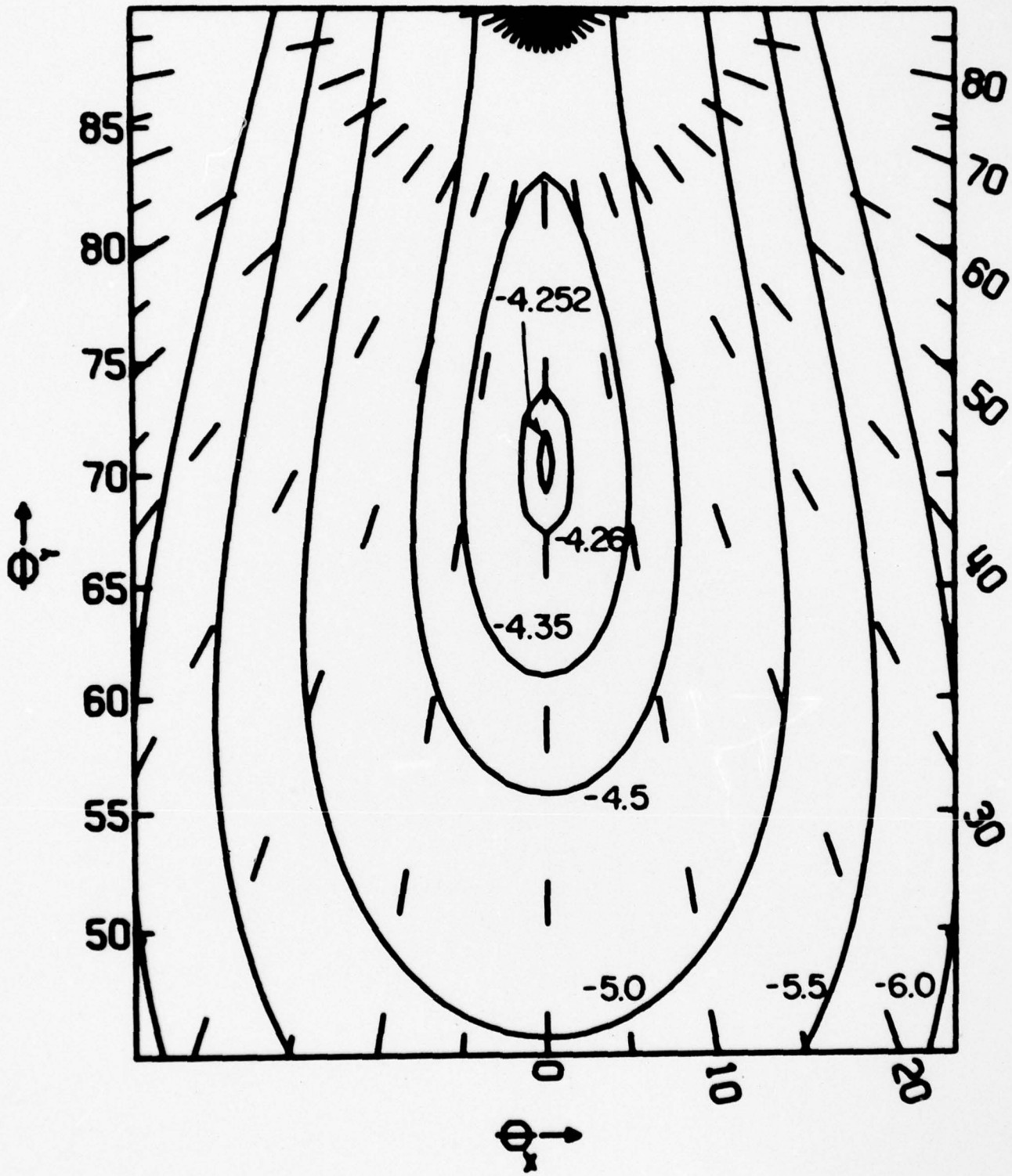
85
80
75
70
65
60
55
50
80
70
60
50
40
30
-4.252
-4.26
-4.35
-4.5
-5.0
-5.5
-6.0
0
10
20
Φ
θ

Figure 7

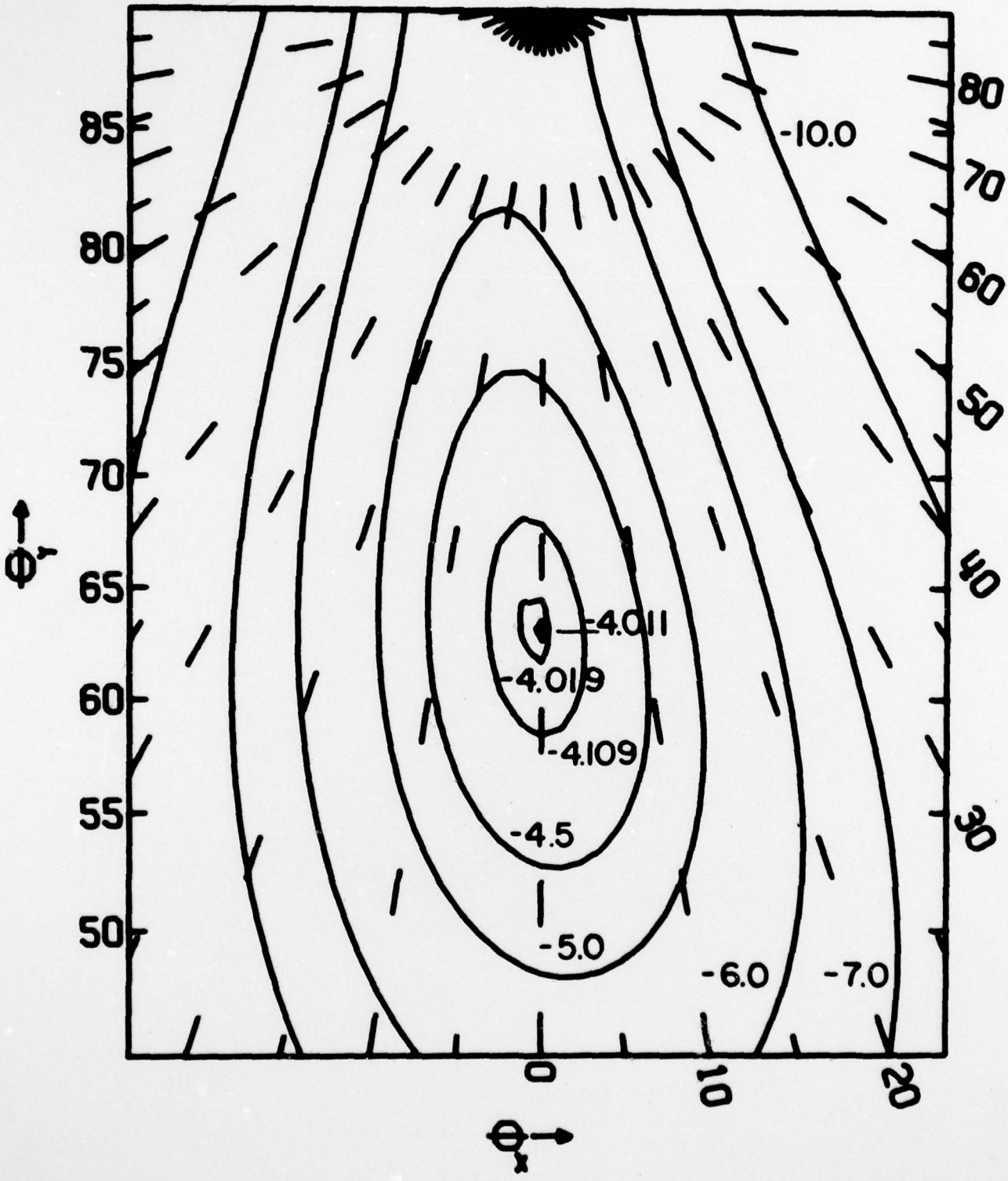
85
80
75
70
65
60
55
50
80
70
60
50
40
30
-10.0
-4.011
-4.019
-4.109
-4.5
-5.0
-6.0
-7.0
0
10
20
ϕ_y
θ_x

Figure 8

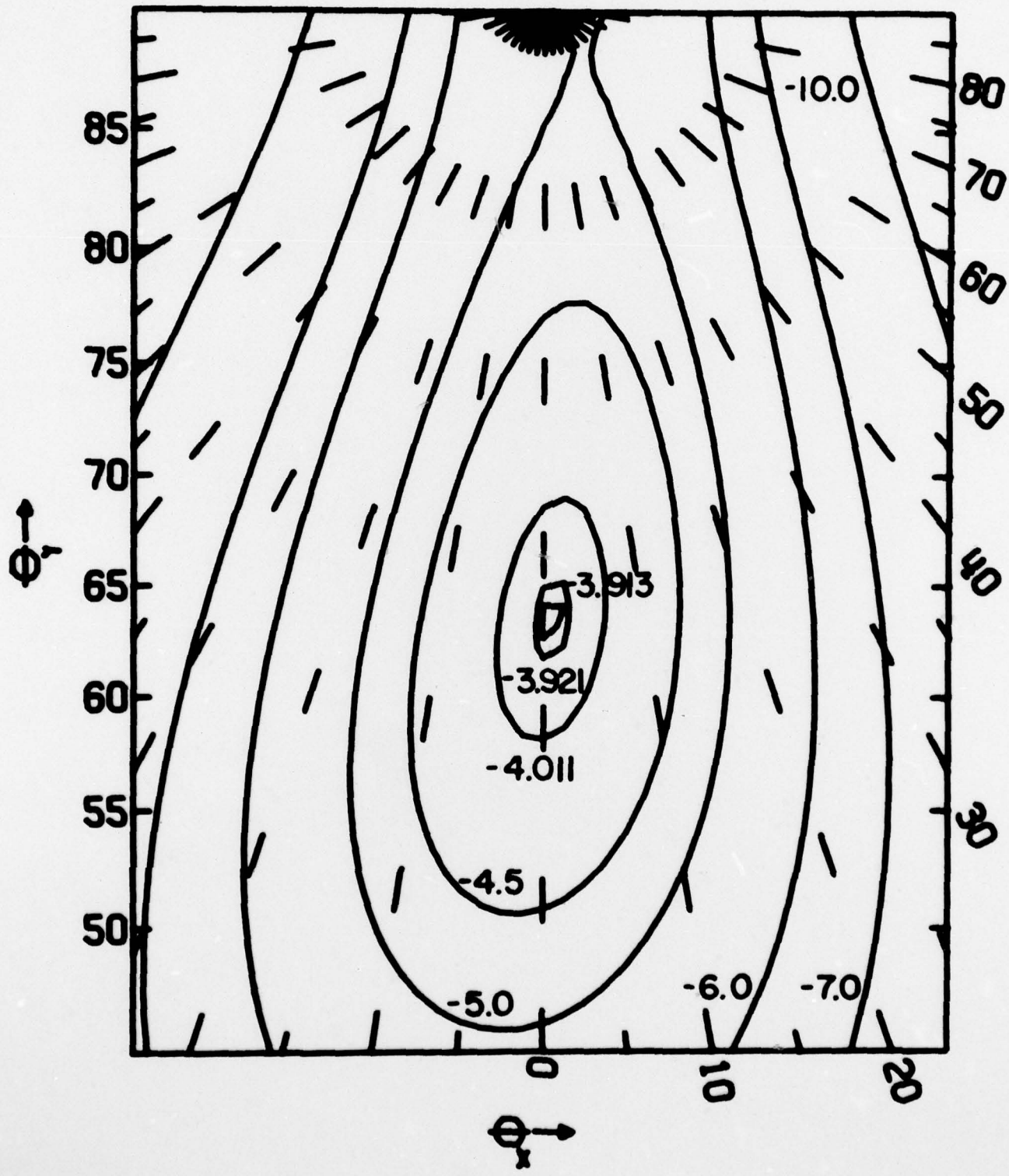
-10.0
-3.913
-3.921
-4.011
-4.5
-5.0
-6.0
-7.0
85
80
75
70
65
60
55
50
80
70
60
50
40
30
0
10
20
Φ_1
Θ_1

Figure 9

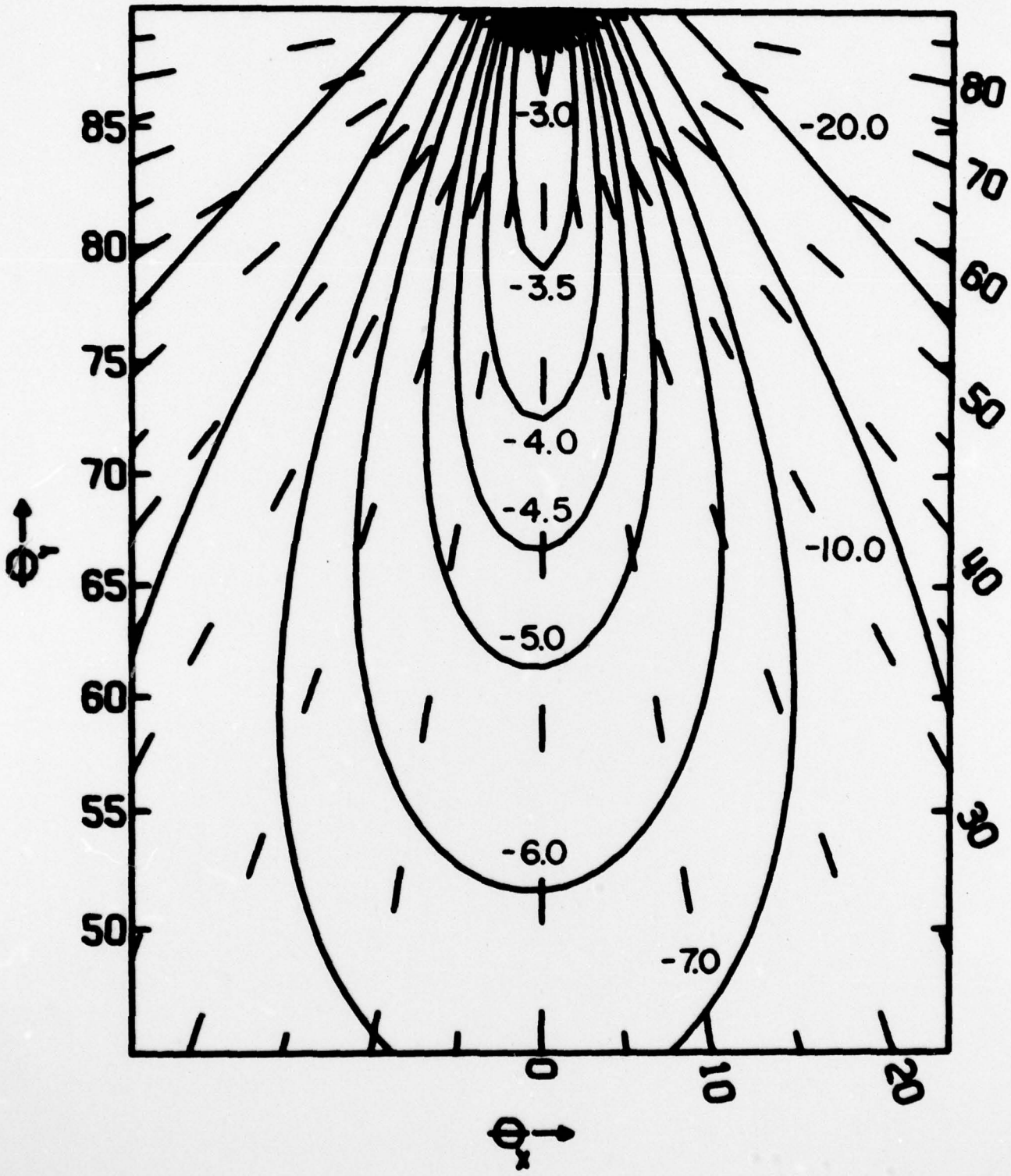
-3.0
-3.5
-4.0
-4.5
-5.0
-6.0
-7.0
-20.0
-10.0
85
80
75
70
65
60
55
50
80
70
60
50
40
30
0
10
20
Φ
θx

Figure 10

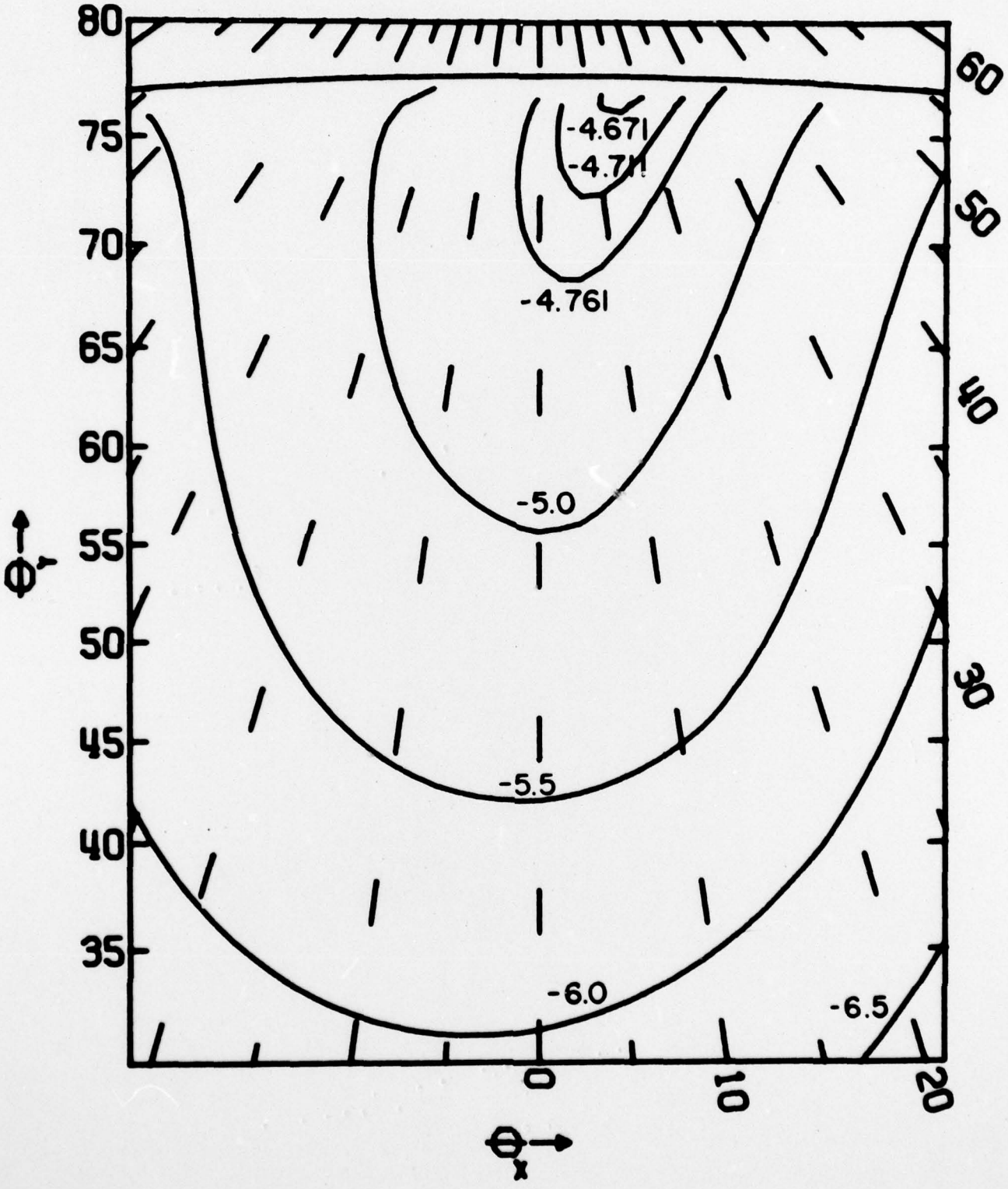
80
75
70
65
60
55
50
45
40
35
60
50
40
30
-4.671
-4.71
-4.761
-5.0
-5.5
-6.0
-6.5
0
10
20
Φ_Y
Θ_X

Figure 11

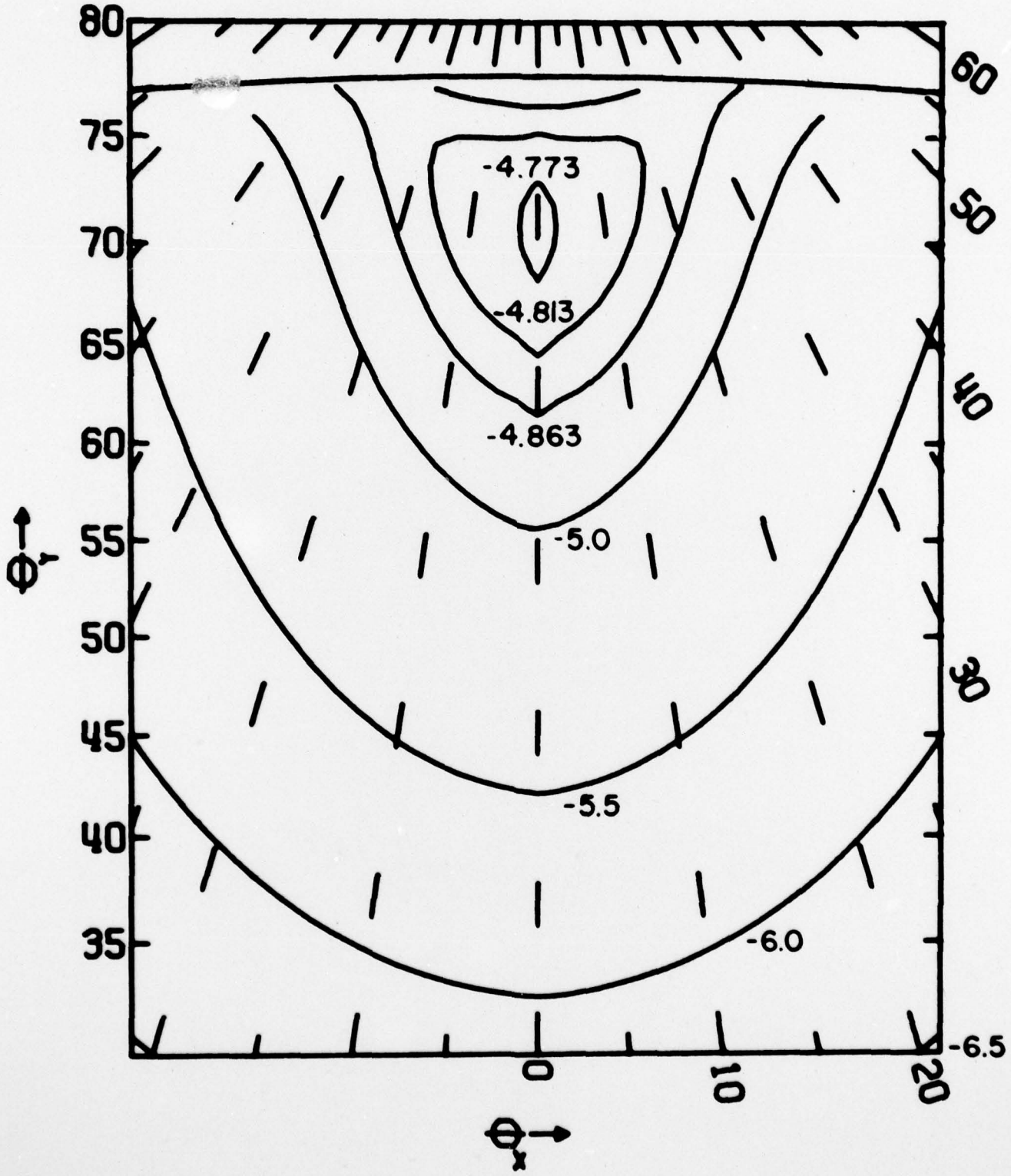
80
75
70
65
60
55
50
45
40
35
60
50
40
30
-6.5
-4.773
-4.813
-4.863
-5.0
-5.5
-6.0
0
10
20
ϕ_y
θ_x

Figure 12

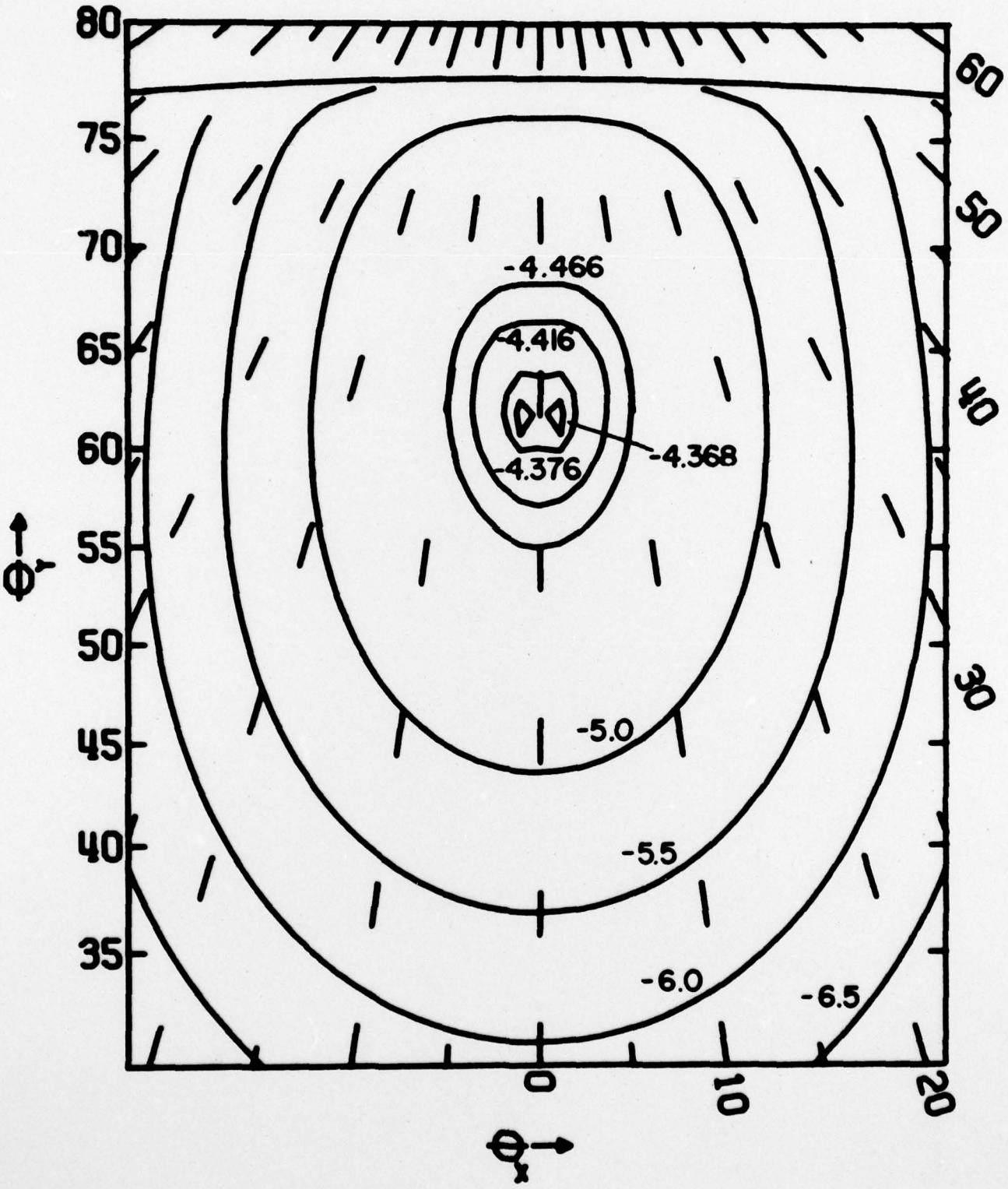
80
75
70
65
60
55
50
45
40
35
60
50
40
30
-4.466
-4.416
-4.376
-4.368
-5.0
-5.5
-6.0
-6.5
0
10
20
ϕ_y
ϕ_x

Figure 13

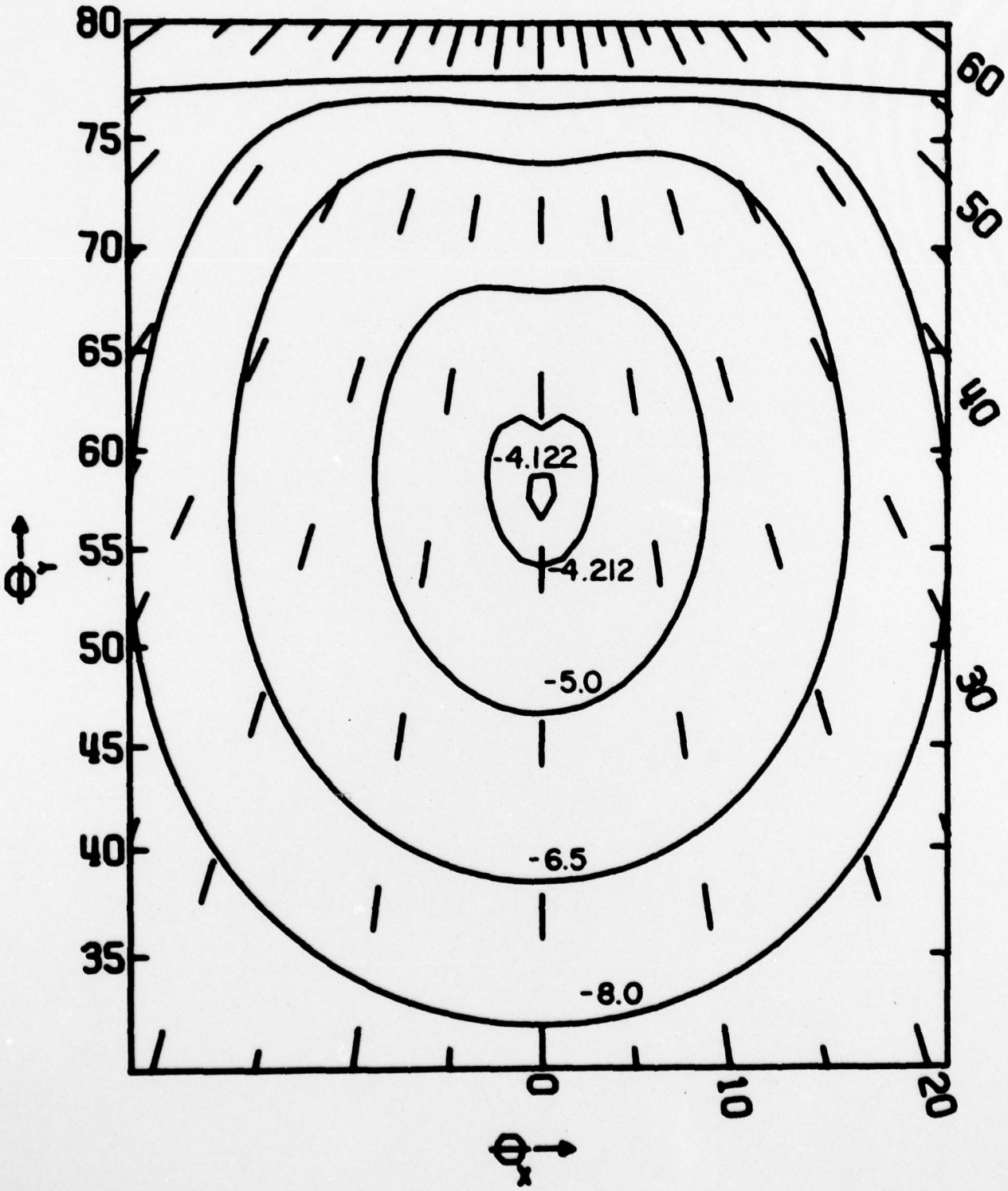
80
75
70
65
60
55
50
45
40
35
60
50
40
30
-4.122
-4.212
-5.0
-6.5
-8.0
0
10
20
ϕ_y
ϕ_x

Figure 14

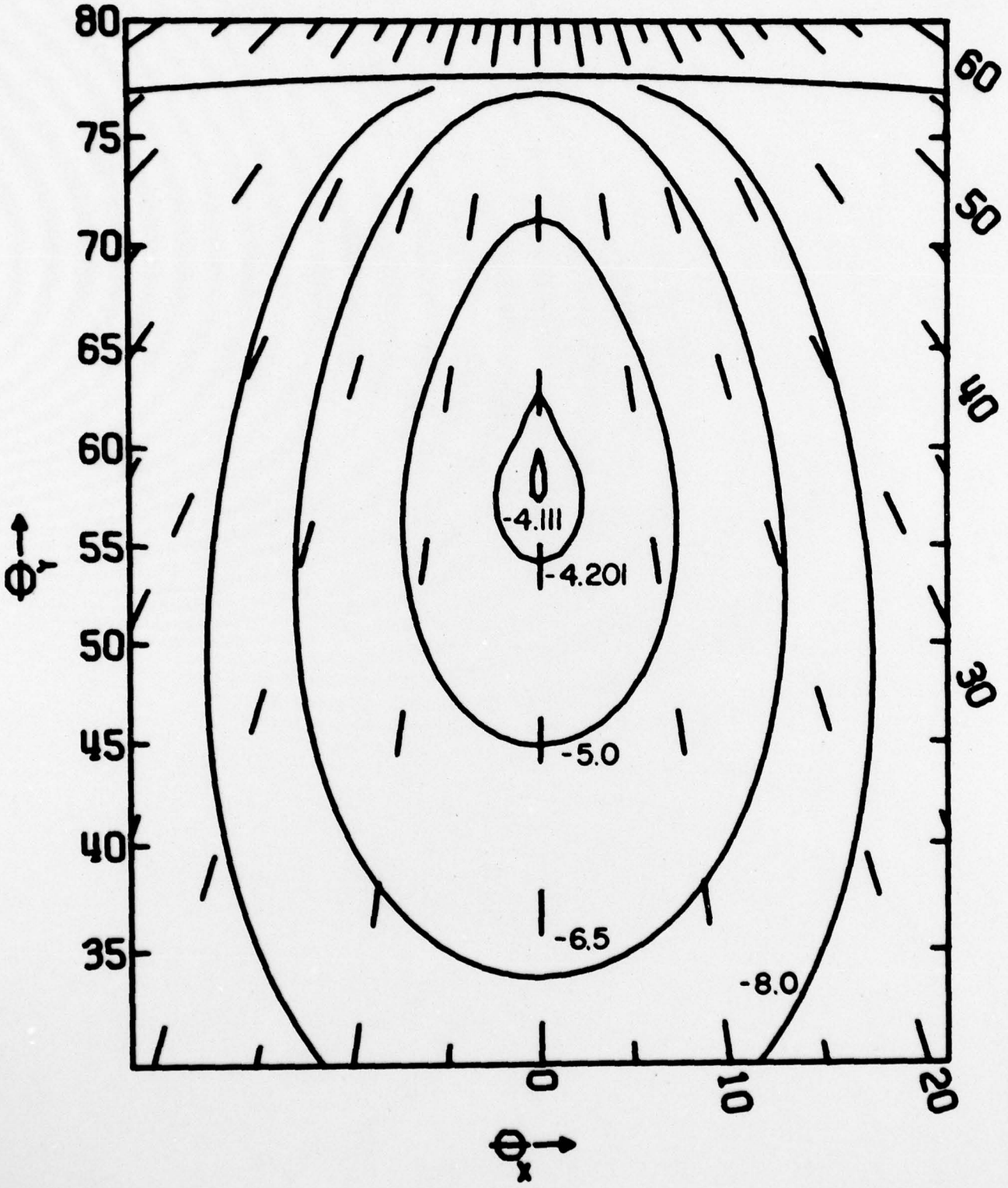
80
75
70
65
60
55
50
45
40
35
60
50
40
30
-4.111
-4.201
-5.0
-6.5
-8.0
0
10
20
Φ_y
θ_x

Figure 15

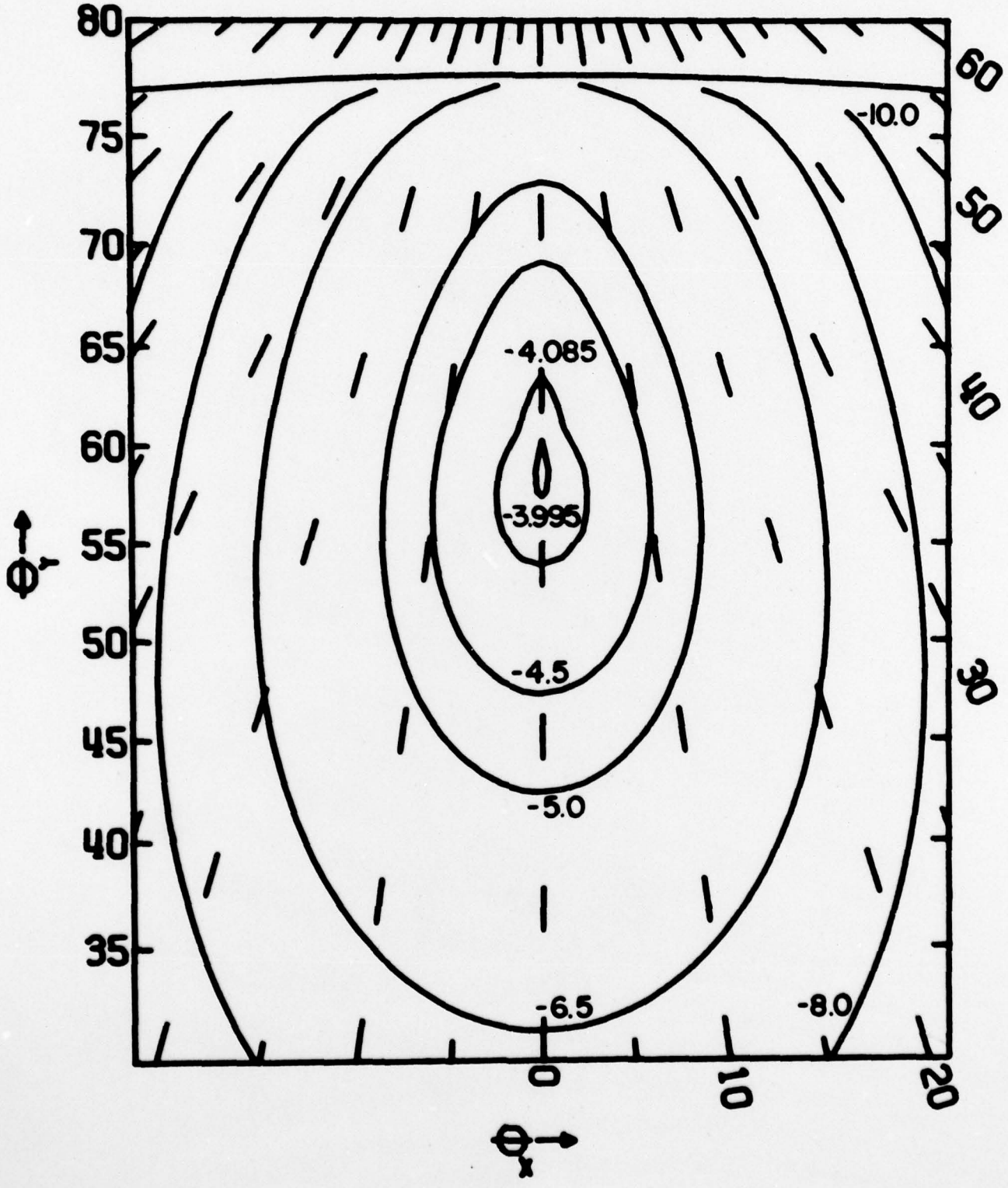
80
75
70
65
60
55
50
45
40
35
60
50
40
30
-10.0
-4.085
-3.995
-4.5
-5.0
-6.5
-8.0
0
10
20
Φ_Y
Θ_X

Figure 16

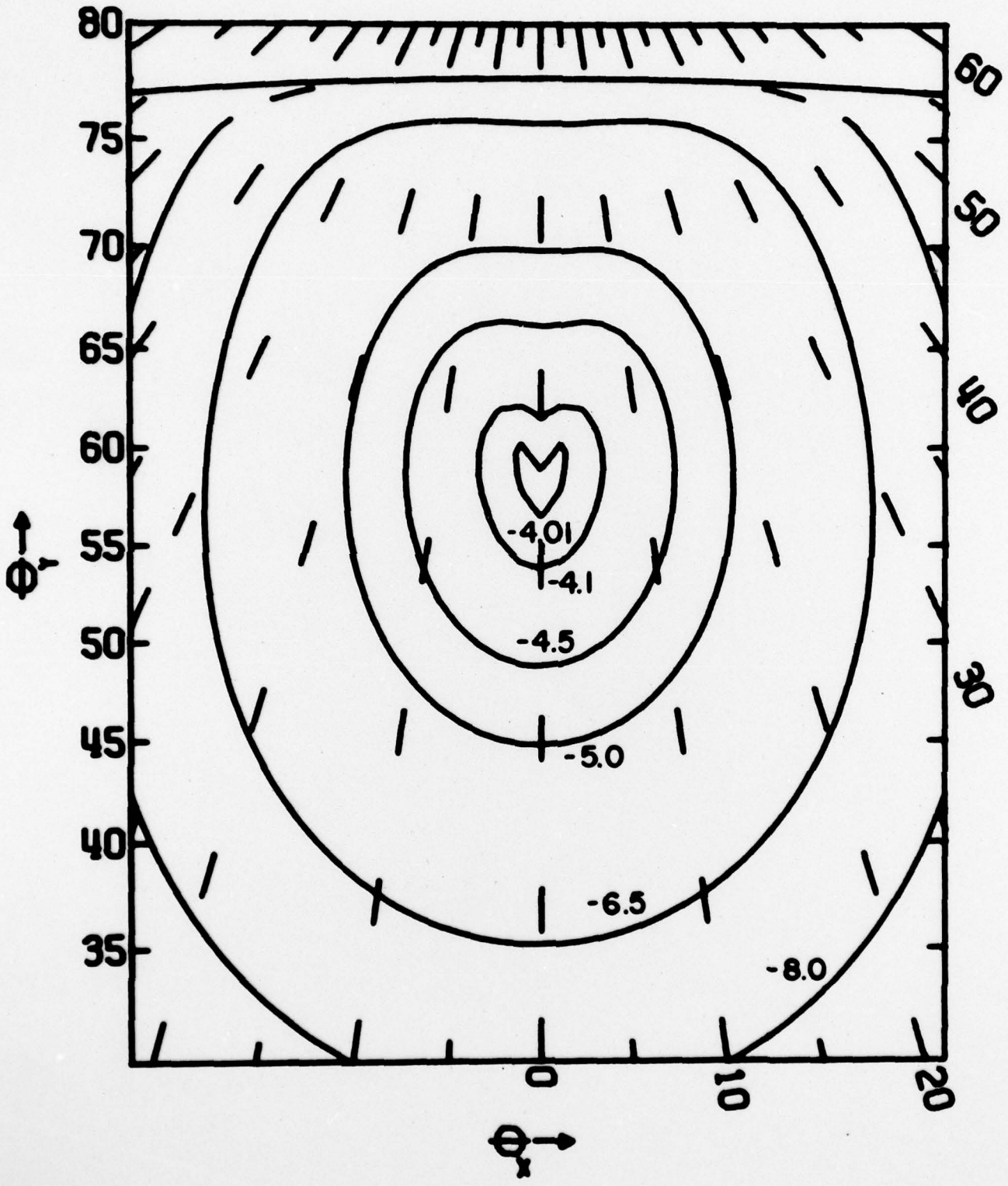
80
75
70
65
60
55
50
45
40
35
60
50
40
30
-4.01
-4.1
-4.5
-5.0
-6.5
-8.0
0
10
20
ϕ_y
θ_x

Figure 17

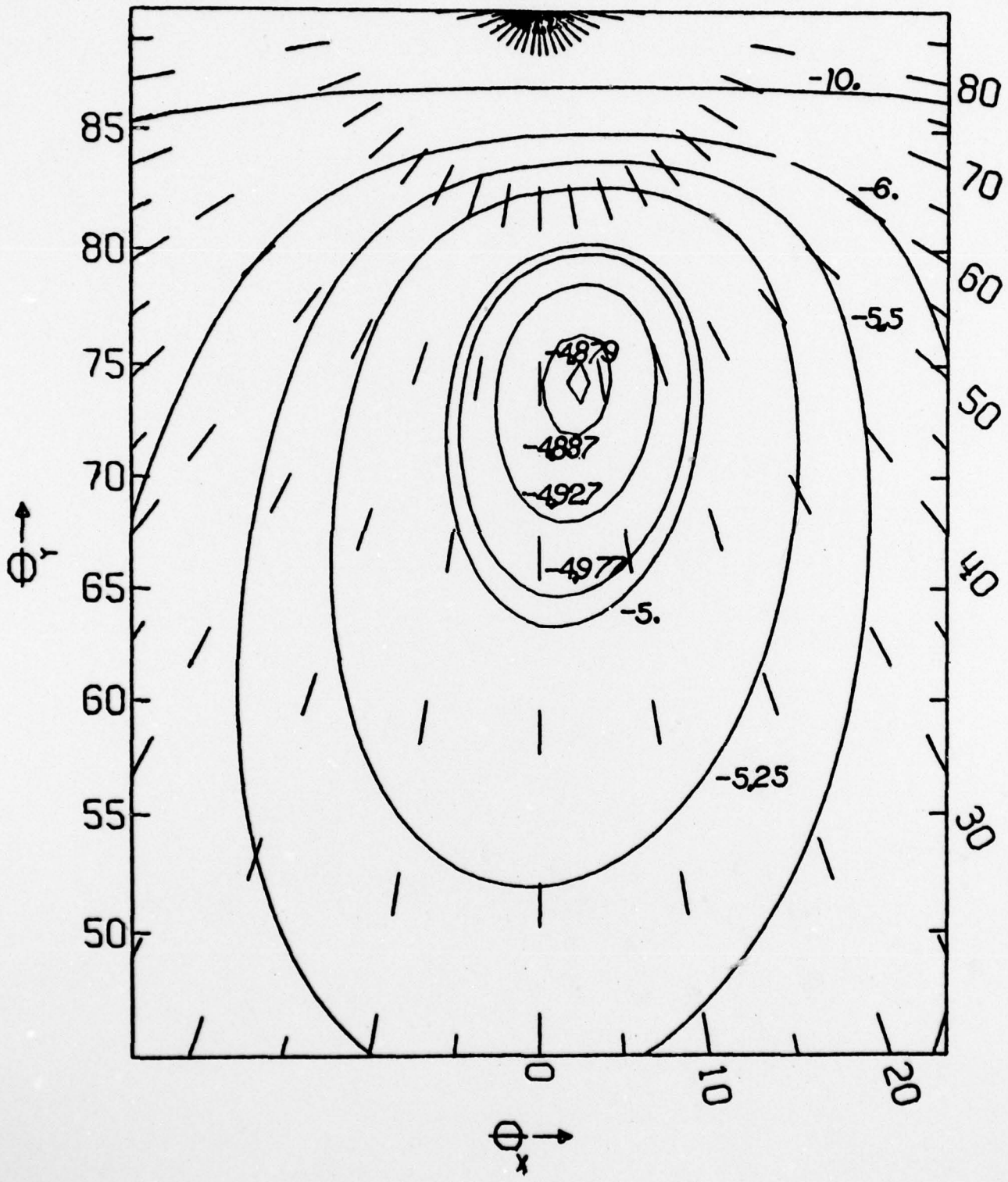
-10.
-6.
-5.5
-4879
-4887
-4927
-497
-5.
-5.25
85
80
75
70
65
60
55
50
80
70
60
50
40
30
0
10
20
ϕ_Y
θ_X

Figure 18

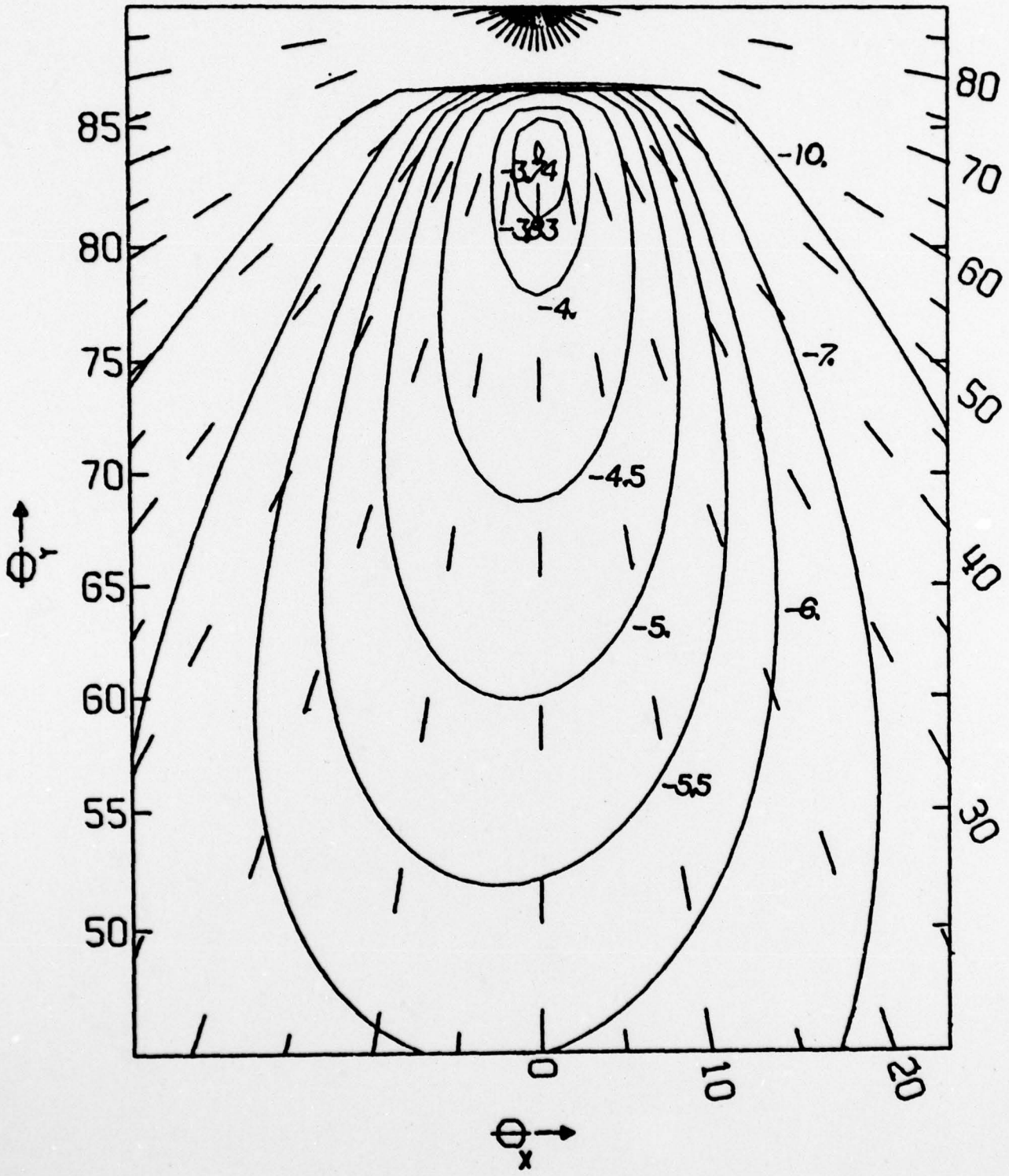
85
80
75
70
65
60
55
50
80
70
60
50
40
30
-10.
-3.4
-3.3
-4.
-7.
-4.5
-6.
-5.
-5.5
0
10
20
Φ_Y
Θ_X

Figure 19

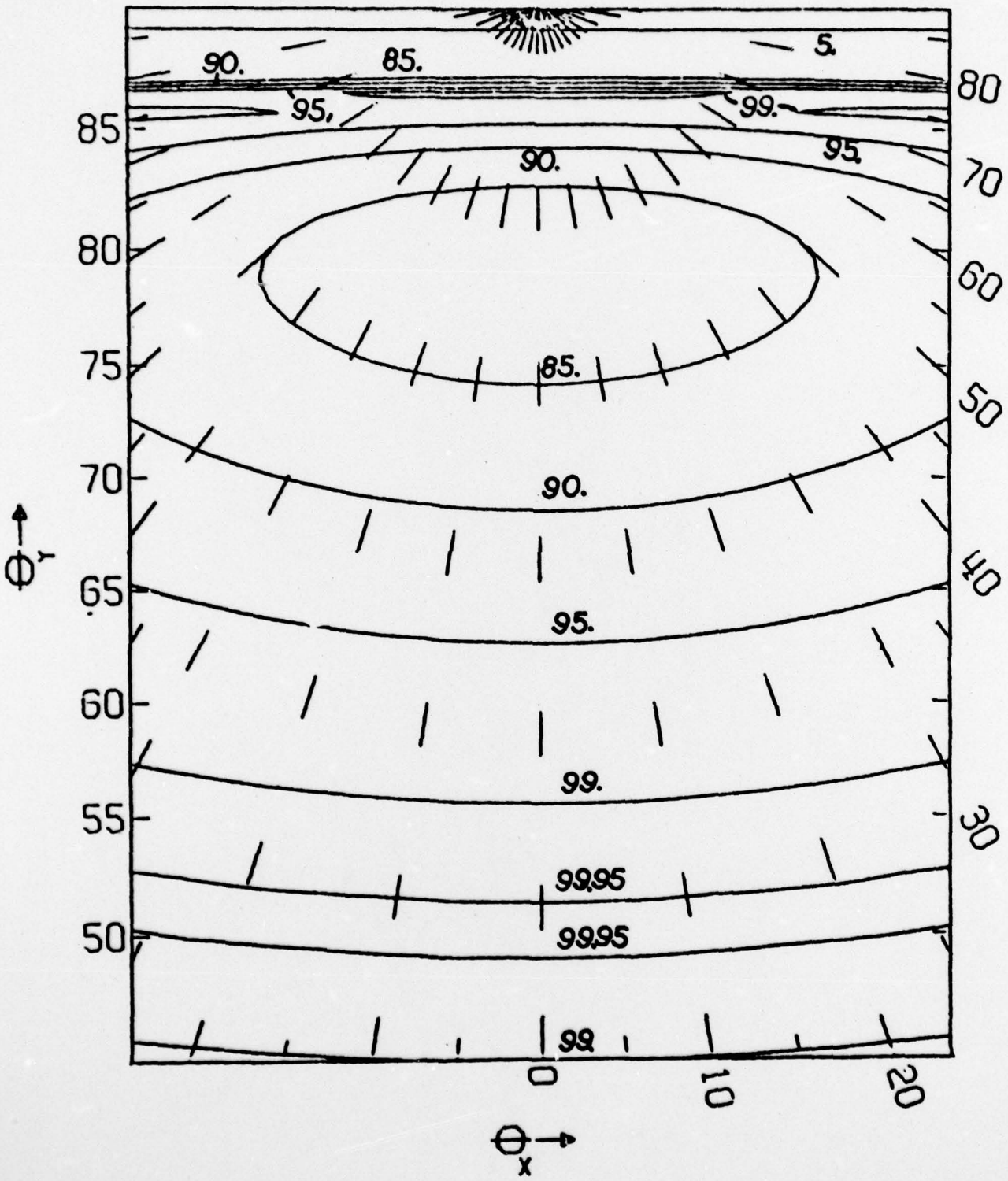
90.
85.
5.
95.
99.
90.
95.
85.
90.
95.
99.
99.95
99.95
99
85
80
75
70
65
60
55
50
80
70
60
50
40
30
0
10
20
Φ_Y
Θ_X

Figure 20

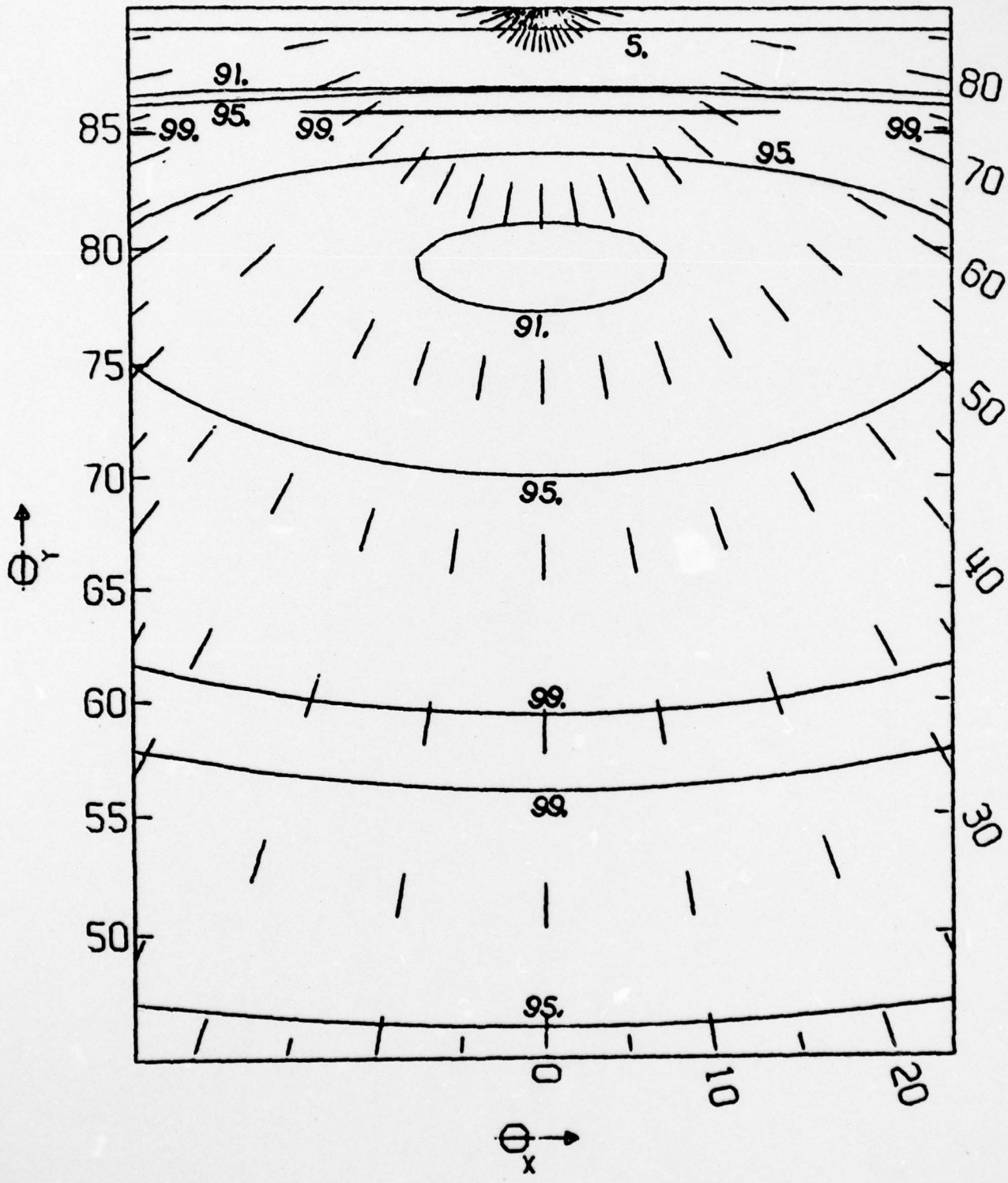
5.
91.
95.
99.
99.
95.
99.
91.
95.
99.
99.
95.
85
80
75
70
65
60
55
50
80
70
60
50
40
30
0
10
20
Φ Y
Θ X

Figure 21